Inorg. Chem. **2003**, *42*, 2311–2322

Structure and Magnetic Properties of Tetraarylporphinatomagnesium(II) Electron Transfer Salts of 2,3,5,6-Tetrafluoro-7,7,8,8-tetracyanoquinodimethane, $TCNQF_4$

Wendy Hibbs,[1a] Atta M. Arif,[1a] Mark Botoshansky,[1b] Menahem Kaftory,[1b] and Joel S. Miller*,[1a]

Department of Chemistry, University of Utah, 315 S. 1400 East RM 2020, Salt Lake City, Utah 84112-0850, and Department of Chemistry, Technion—Israel Institute of Technology, Haifa, 32000 Israel

Received August 5, 2002

The crystal structures of the 2,3,5,6-tetrafluoro-7,7,8,8-tetracyanoquinodimethane, $TCNQF_4$, electron transfer salts of *meso*-tetraphenylporphinatomagnesium(II), [MgTPP][$TCNQF_4$]·PhMe and [MgTPP][$TCNQF_4$]·3(1,2-$C_6H_4Cl_2$), and *meso*-tetrakis(3,4,5-trimethoxyphenyl)porphinatomagnesium(II), [MgT(3,4,5-OMe)PP][$TCNQF_4$]·3(1,2-$C_6H_4Cl_2$), provide the first structurally characterized examples of 1-D metal–radical chains involving [Mg^{II}(porphyrin$^{\bullet}$)]$^+$. These salts possess [$TCNQF_4$]$^{\bullet-}$ stabilized by *trans*-μ-coordination to Mg(II) and exhibit ν_{CN} at 2199 and 2177, 2212 and 2187, and 2194 and 2172 cm^{-1}, respectively. The [$TCNQF_4$]$^{\bullet-}$ species is planar and bridges two cations with MgN distances of 2.266(16), 2.221(2), and 2.276(3) Å, respectively, which are shorter than the MnN 2.321(3) Å distance observed for [MnT(3,4,5-OMe)PP][$TCNQF_4$]·3(1,2-$C_6H_4Cl_2$). The room-temperature effective moments for [MgTPP][$TCNQF_4$]·*x*S (S = PhMe and 1,2-$C_6H_4Cl_2$) and [MgTPP][$C_4(CN)_6$]·PhMe are consistent with the calculated spin only value of 2.45 μ_B with weak antiferromagnetic coupling ($J_{intra}/k_B \sim -2.9$ K; $H = -2J\mathbf{S_a}\cdot\mathbf{S_b}$) for these [$TCNQF_4$]$^{\bullet-}$ salts and for this [$C_4(CN)_6$]$^{\bullet-}$ salt ($J_{intra}/k_B \sim -0.8$ K) on the basis of fits to several models. The coupling is significantly reduced with respect to that of the Mn analogues due to lack of spin on the metal site for [Mg^{II}(por$^{\bullet}$)]$^+$. The antiferromagnetic coupling is enhanced for [MgT(3,4,5-OMe)PP][$TCNQF_4$] with respect to [MgTPP][$TCNQF_4$] as [$TCNQF_4$]$^{\bullet-}$ gets closer to the [Mg^{II}(por$^{\bullet}$)]$^+$ plane, which leads to greater interactions and coupling.

Introduction

The study of magnetically ordered molecule-based materials is a growing area of contemporary chemistry.[2,3] [$Fe(C_5Me_5)_2$]$^{\bullet+}$[TCNE]$^{\bullet-}$ (TCNE = tetracyanoethylene) was the first organic-containing molecule-based magnet characterized, and it has an ordering temperature, T_c, of 4.8 K.[4] Improvements led to the discovery of V(TCNE)$_x$·*y*(solvent), the first room-temperature organic magnet ($T_c \sim 400$ K),[5] and later the magnetically ordered Mn,[6a] Fe,[6] Ni,[6a] and Co[6a] analogues. More recently, studies have focused on a class of metallomacrocycles and organic radical-based magnets

* To whom corrrespondence should be addressed. E-mail: jsmiller@chem.utah.edu.

(1) (a) University of Utah. (b) Technion.

(2) (a) Proceedings on the Conference on Ferromagnetic and High Spin Molecular Based Materials: Miller, J. S., Dougherty D., Eds. *Mol. Cryst. Liq. Cryst.* **1989**, *176*. (b) Proceedings on the Conference on Molecular Magnetic Materials: Kahn, O., Gatteschi, D., Miller, J. S., Palacio, F., Eds. *NATO ARW Molecular Magnetic Materials* **1991**, *E198*. (c) Proceedings on the Conference on the Chemistry and Physics of Molecular Based Magnetic Materials: Iwamura, H., Miller, J. S., Eds. *Mol. Cryst. Liq. Cryst.* **1993**, *232/233*. (d) Proceedings on the Conference on Molecule-Based Magnets: Miller, J. S., Epstein, A. J., Eds. *Mol. Cryst. Liq. Cryst.* **1995**, *271−274*. (e) Proceedings on the Conference on Molecular-Based Magnets: Itoh, K., Miller, J. S., Takui, T., Eds. *Mol. Cryst. Liq. Cryst.* **1997**, *305/306*. (f) Turnbull, M. M., Sugimoto, T., Thompson, L. K., Eds. *ACS Symp. Ser.* **1996**, *644*.

(3) Reviews: (a) Miller, J. S.; Epstein, A. J. *Chem. Commun.* **1998**, 1319. (b) Ovcharenko, V. I.; Sagdeev, R. Z. *Russ. Chem. Rev.* **1999**, *68*, 345. (c) Plass, W. *Chem. Ztg.* **1998**, 32, 323. (d) Miller, J. S.; Epstein, A. J. *Chem. Eng. News*, **1995**, *73* (40), 30. (e) Miller, J. S.; Epstein, A. J. *Angew. Chem., Int. Ed. Engl.* **1994**, *33*, 385. (f) Kinoshita, M. *Jpn. J. Appl. Phys.* **1994**, *33*, 5718. (g) Miller, J. S.; Epstein, A. J. *Adv. Chem. Ser.* **1995**, *245*, 161. (h) Caneschi, A.; Gatteschi, D. *Prog. Inorg. Chem.* **1991**, *37*, 331. (i) Buchachenko, A. L. *Russ. Chem. Rev.* **1990**, *59*, 307. (j) Kahn, O. *Struct. Bonding (Berlin)* **1987**, *68*, 89. (k) Caneschi, A.; Gatteschi, D.; Sessoli, R.; Rey, P. *Acc. Chem. Res.* **1989**, *22*, 392. (l) Gatteschi, D. *Adv. Mater.* **1994**, *6*, 635. (m) Miller, J. S.; Epstein, A. J.; Reiff, W. M. *Acc. Chem. Res.* **1988**, *21*, 114. (n) Miller, J. S.; Epstein, A. J.; Reiff, W. M. *Science* **1988**, *240*, 40. (o) Miller, J. S.; Epstein, A. J.; Reiff, W. M. *Chem. Rev.* **1988**, *88*, 201. (p) Miller, J. S.; Epstein, A. J. In *New Aspects of Organic Chemistry*; Yoshida, Z., Shiba, T., Oshiro, Y., Eds.; VCH Publishers: New York, 1989; p 237.

(4) Miller, J. S.; Calabrese, J. C.; Epstein, A. J.; Bigelow, R. W.; Zhang, J. H.; Reiff, W. M. *J. Chem. Soc., Chem. Commun.* **1986**, 1026. Miller, J. S.; Calabrese, J. C.; Rommelmann, H.; Chittipeddi, S.; Zhang, J. H.; Reiff, W. M.; Epstein, A. J. *J. Am. Chem. Soc.* **1987**, *109*, 769.

10.1021/ic020494w CCC: $25.00
Published on Web 03/05/2003

such as [MnTPP][TCNE]·2PhMe (H_2TPP = *meso*-tetraphenylporphyrin).[3a,7] A wide range of manganese porphyrin compounds have been structurally characterized with $[TCNE]^{\bullet-}$ *trans*-μ-N-σ-bound to Mn^{III} forming a 1-D coordination polymer consisting of parallel chains of alternating $\cdots D^{\bullet+}A^{\bullet-}D^{\bullet+}A^{\bullet-}\cdots$ (D = MnTPP; A = radical anion).[3a] These materials are ferrimagnets resulting from the antiferromagnetic coupling of the $S = 2$ Mn^{III} with $S = {}^1/_2$ $[TCNE]^{\bullet-}$ with critical temperatures, T_c's, ranging from 3.5 to 28 K.[3a,8] Furthermore, at low temperature they exhibit complex magnetic behaviors that include large coercivities in the range of 27 kOe.[9]

Studies have primarily focused upon the reaction of $S = {}^5/_2$ *meso*-tetraphenylporphinatomanganese(II) with strong electron acceptors such as TCNE, 7,7,8,8-tetracyano-*p*-quinodimethane (TCNQ), 2,3-dichloro-5,6-dicyanobenzoquinone (DDQ), $C_4(CN)_6$, and 2,3,5,6-tetrafluoro-7,7,8,8-tetracyano-*p*-quinodimethane ($TCNQF_4$). For $[TCNE]^{\bullet-}$-based materials, antiferromagnetic coupling is attributed to the σ overlap of the Mn d_{z^2} orbital and the $[TCNE]^{\bullet-}$ π_z orbital.[10] Herein, we extend the studied systems to Mg^{II}(por) (por = porphyrin), which unlike Mn^{II}(por) does not possess an easily oxidizable metal center, and oxidation occurs on the porphyrin ring producing a π-cation radical, i.e., $[Mg^{II}(por^{\bullet})]^+$.[11] Interaction between the unpaired electrons on the $por^{\bullet+}$ and radical anion could lead to a ferromagnetic interaction, as these spins potentially reside in orthogonal orbitals if they are perpendicular to each other. The first ring oxidation potential of Mg^{II}(por) ($E^\circ_{1/2} = 0.54$ V in MeCN vs SCE)[11a] is 0.91 V greater than the $Mn^{II/III}$ oxidation potential ($E^\circ_{1/2} = -0.37$ V in MeCN vs SCE)[11b] and, hence, requires an oxidizing agent stronger than TCNE ($E^\circ_{1/2} = 0.15$ V in MeCN vs SCE). $TCNQF_4$ ($E^\circ_{1/2} = 0.53$ V in MeCN vs SCE)[12] and $C_4(CN)_6$ ($E^\circ_{1/2} = 0.60$ V in MeCN vs SCE)[12] are strong acceptors that have reduction potentials sufficient to oxidize the porphyrin ring. It should be noted that ring oxidation for Cu^{II}TPP (0.90 V)[11a] and Ni^{II}TPP (1.05 V)[11a] requires even stronger oxidizing agents, Table 1, and, consequently, was not studied.

Table 1. Electrochemical Potentials of Metalloporphyrins and Electron Acceptors, $E^\circ_{1/2}$ vs SCE in 0.1 M $[n\text{-}Bu_4N][PF_6]$[11,12]

M(por)	first ring oxidn, V	M^{II}/M^{III}, V	acceptor	redn, V
MnTPP[a]	1.32	−0.37	TCNE[b]	0.15
MgTPP[b]	0.54		TCNQ[b]	0.17
CuTPP[b]	0.90		$TCNQF_4$[b]	0.53
NiTPP[a]	1.05	1.15	$C_4(CN)_6$[b]	0.60

[a] MeCN. [b] CH_2Cl_2.

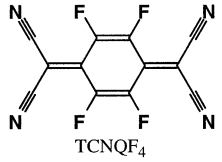

$TCNQF_4$

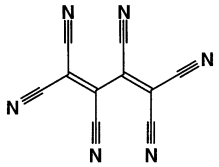

$C_4(CN)_6$

Experimental Section

Synthesis. Solvents used in the preparation of magnesium porphyrins were used as received. Solvents used for preparation of the electron transfer salts were distilled under nitrogen from appropriate drying agents before use, and the syntheses of electron transfer salts were carried out in inert atmosphere DriLab or using standard Schlenk vacuum techniques. $TCNQF_4$ was obtained as a gift from the Du Pont Co. and was recrystallized from CH_2Cl_2 prior to use. $C_4(CN)_6$ was synthesized according to a modified[13a] literature procedure.[13b] Pyrrole was dried by vacuum distillation from CaH_2. The substituted liquid benzaldehydes were purified by distillation and solid benzaldehydes recrystallized from toluene.

All free-base porphyrins were prepared by the Adler−Longo method that involves refluxing pyrrole and the appropriately substituted benzaldehyde in propionic acid for 30 min.[14] Chlorin impurities were removed via the metalation of the corresponding free-base porphyrins. Relative purity was confirmed by thin-layer chromatography and/or UV−vis spectroscopy. The free-base porphyrins were metalated according to the literature[15] method by reaction with MgI_2[16] in dichloromethane stabilized with triethylamine. The products were purified via boiling in toluene to remove the triethylamine and then recrystallized from CH_2Cl_2/MeOH. MgTPP was further purified by dynamic vacuum sublimation at 325 °C and 50 mTorr.

[MgTPP][TCNQF$_4$]·PhMe, 1a. MgTPP (31.9 mg, 0.0500 mmol) was dissolved upon stirring in 15 mL of hot toluene (∼110 °C). The purple solution was filtered through a medium-frit funnel. To this was added a filtered solution of $TCNQF_4$ (13.8 mg, 0.0500 mmol) dissolved in 15 mL hot toluene in a 50 mL flask. The flask was capped and stirred for 24 h without heating to prevent precipitation of $TCNQF_4$. After 24 h, the solvent volume was

(5) (a) Manriquez, J. M.; Yee, G. T.; McLean, R. S.; Epstein, A. J.; Miller, J. S. *Science* **1991**, *252*, 1415. (b) Epstein, A. J.; Miller, J. S. In *Conjugated Polymers and Related Materials: The Interconnection of Chemical and Electronic Structure*; Proceedings of Nobel Symposium #NS-81; Oxford University Press: Oxford, 1993; p 475; *La Chim. La Ind.* **1993**, *75*, 185, 257. (c) Miller, J. S.; Yee, G. T.; Manriquez, J. M.; Epstein, A. J. In *Conjugated Polymers and Related Materials: The Interconnection of Chemical and Electronic Structure*; Proceedings of Nobel Symposium #NS-81; Oxford University Press: Oxford, 1993, p 461; *La Chim. La Ind.* **1992**, *74*, 845.
(6) (a) Zhang, J. H.; Ensling, J.; Ksenofontov, V.; Gütlich, P.; Epstein, A. J.; Miller, J. S. *Angew. Chem., Int. Ed.* **1998**, *37*, 657. (b) Pokhodnya, K. I.; Petersen, N.; Miller, J. S. *Inorg. Chem.* **2002**, *41*, 1996.
(7) (a) Miller, J. S.; Calabrese, J. C.; McLean, R. S.; Epstein, A. J. *Adv. Mater.* **1992**, *4*, 498. (b) Zhou, P.; Morin, B. G.; Epstein, A. J.; McLean, R. S.; Miller, J. S. *J. Appl. Phys.* **1993**, *73*, 6569. Brinckerhoff, W. B.; Morin, B. G.; Brandon, E. J.; Miller, J. S.; Epstein, A. J. *J. Appl. Phys.* **1996**, *79*, 6147.
(8) Rittenberg, D. K.; Miller, J. S. *Inorg. Chem.* **1999**, *38*, 4838.
(9) Rittenberg, D. K.; Sugiura, K.-i.; Sakata, Y.; Mikami, S.; Epstein, A. J.; Miller, J. S. *Adv. Mater.* **2000**, *12*, 126.
(10) Brandon, E. J.; Kollmar, C.; Miller, J. S. *J. Am. Chem. Soc.* **1998**, *120*, 1822.
(11) (a) Felton, R. H. *The Porphyrins: Physical Chemistry, Part C*; Dolphin, D., Ed.; Academic Press: New York, 1978; Vol. 5, pp 58−9. (b) Kelly, S. L.; Kadish, K. M. *Inorg. Chem.* **1982**, *21*, 3631.
(12) Ward, M. D. In *Electroanalytical Chemistry: A Series of Advances;* Bard, A. J., Ed.; Marcel Dekker: New York, 1989; Vol. 16, pp 181−299.
(13) (a) In lieu of a literature method for extracting $C_4(CN)_6$ from NaBr with dioxane, acetonitrile was used to dissolve $C_4(CN)_6$, and NaBr was collected by filtration. The solution was brought to dryness, and $C_4(CN)_6$ was purified by vacuum sublimation at 130 °C. (b) Webster, O. W. *J. Am. Chem. Soc.* **1964**, *86*, 2898.
(14) Adler, A. D.; Longo, F. R.; Finarelli, J. D.; Goldmacher, J.; Assour, J.; Korsakoff, L. *J. Org. Chem.* **1967**, *32*, 476.
(15) Lindsey, J. S.; Woodford, J. N. *Inorg. Chem.* **1995**, *34*, 1063.
(16) Prepared in situ by reaction of excess Mg (Strem, 99.8% pure) with I_2 in diethyl ether with stirring until solution was colorless. Excess Mg was filtered off, and solution was brought to dryness yielding white MgI_2.

reduced to 5 mL to induce precipitation of the product. The resulting purple precipitate was collected via vacuum filtration and washed with 10 mL of toluene. TGA: 7.9% weight loss below 149 °C attributed to the solvent ($x = 0.85$ PhMe). IR (Nujol, ν_{CN}): 2199 (s), 2177 (m) cm^{-1}.

[MgTPP][TCNQF$_4$]·3(1,2-C$_6$H$_4$Cl$_2$), 1b. MgTPP (31.9 mg, 0.0500 mmol) was dissolved with stirring in 15 mL of hot 1,2-dichlorobenzene. The purple solution was filtered through a medium-frit funnel. To this was added a filtered solution of $TCNQF_4$ (13.8 mg, 0.0500 mmol) dissolved in 15 mL of hot 1,2-dichlorobenzene in a 50 mL flask. The solution was allowed to sit overnight, and the resulting shiny purple crystals were collected via vacuum filtration and washed with 10 mL of 1,2-dichlorobenzene. TGA: 32.2% weight loss below 152 °C attributed to the solvent ($x = 2.95$ 1,2-$C_6H_4Cl_2$). IR (Nujol, ν_{CN}): 2212 (s), 2187 (m) cm^{-1}.

[MgT(3,4,5-OMe)PP][TCNQF$_4$]·3(1,2-C$_6$H$_4$Cl$_2$), 2. MgT(3,4,5-OMe)PP (49.9 mg, 0.0500 mmol) was dissolved with stirring in 15 mL of hot 1,2-dichlorobenzene. The purple solution was filtered through a medium-frit funnel. To this was added a filtered solution of $TCNQF_4$ (13.8 mg, 0.0500 mmol) dissolved in 15 mL of hot 1,2-dichlorobenzene in a 50 mL flask. The solution was allowed to cool, and a minimal amount of hexane was added to induce precipitation. Purple crystals formed, and they were collected via vacuum filtration, washed with 10 mL of 1,2-dichlorobenzene, and dried in vacuo. TGA: 21.5% weight loss below 112 °C attributed to the solvent ($x = 2.37$ 1,2-$C_6H_4Cl_2$). IR (Nujol, ν_{CN}): 2194 (s), 2172 (m) cm^{-1}.

[MgTPP][C$_4$(CN)$_6$]·*x*PhMe, 3. MgTPP (31.9 mg, 0.0500 mmol) was dissolved with stirring in 20 mL of hot toluene. The purple solution was filtered through a medium-frit funnel. To this was added a filtered solution of $C_4(CN)_6$ (10.2 mg, 0.0500 mmol) dissolved in 20 mL of hot toluene in a 50 mL flask. The solution was allowed to sit overnight, and the resulting shiny purple needlelike crystals were collected via vacuum filtration, washed with 10 mL of toluene, and dried in vacuo. TGA: no weight loss was observed (i.e., $x = 0$ PhMe). Elemental analysis observed for [MgTPP][$C_4(CN)_6$] (calculated for $C_{54}H_{28}MgN_{10}$): C 76.21 (77.10)%, H 3.54 (3.36)%, N 16.15 (16.65)%. See Discussion section for details regarding TGA and elemental analysis. IR (Nujol, ν_{CN}): 2210 (m), 2185 (s) cm^{-1}.

[MgT(3,4,5-OMe)PP][C$_4$(CN)$_6$]·*x*(1,2-C$_6$H$_4$Cl$_2$), 4. MgT(3,4,5-OMe)PP (31.9 mg, 0.0500 mmol) was dissolved with stirring in 20 mL of hot 1,2-dichlorobenzene. The purple solution was filtered through a medium-frit funnel. To this was added a filtered solution of $C_4(CN)_6$ (10.2 mg, 0.0500 mmol) dissolved in 20 mL of hot 1,2-dichlorobenzene in a 50 mL flask. The solution was allowed to cool, and a minimal amount of hexane was added to induce precipitation. The purple microcrystalline material that formed was collected via vacuum filtration, washed with 10-mL of 1,2-dichlorobenzene, and dried in vacuo. TGA: 17% weight loss below 80 °C attributed to the solvent ($x = 1.67$ 1,2-$C_6H_4Cl_2$). Elemental analysis observed for [MgT(3,4,5-OMe)PP][$C_4(CN)_6$]·2.3(1,2-$C_6H_4Cl_2$) (calculated): C 62.24 (62.25)%, H 3.99 (4.01)%, N 9.09 (9.10)%. IR (Nujol, ν_{CN}): 2218 (m), 2183 (s) cm^{-1}.

Physical Methods. The thermal properties were studied on a TA Instruments model 2050 thermogravimetric analyzer (TGA) equipped with a TA-MS Fison triple filter quadrupole mass spectrometer, to identify gaseous products with masses less than 300 amu. This instrument is located in a Vacuum Atmospheres DriLab under argon to protect air and moisture sensitive samples. Samples were placed in an aluminum pan and heated at 20 °C/min under a continuous 10-mL/min nitrogen flow. Elemental analyses were performed by Complete Analysis Laboratories, Inc., Parsippany, NJ, and Atlantic Microlab, Norcross, GA. The 2−300 K magnetic susceptibility was determined on a Quantum Design MPMS-5XL 5 T SQUID (sensitivity = 10^{-8} emu or 10^{-12} emu/Oe at 1 T) as previously described.[17] Due to the large diamagnetic component of the observed magnetization, all magnetic measurements were perform in closed non-air-tight gelatin capsules, allowing for minimal solvent loss during these studies. This solvent loss was accounted for in data calculations. In addition to correcting for the diamagnetic contribution from the sample holder, core diamagnetic corrections of −423, −639, −126, −162, −65.9, and -84.3×10^{-6} emu/mol based on summing Pascal's constants were used for MgTPP, MgT(3,4,5-OMe)PP, $TCNQF_4$, $C_4(CN)_6$, toluene, and 1,2-dichlorobenzene, respectively. The magnetic purity was determined by measuring the magnetic susceptibility according to the Honda−Owen method.[18] After sublimation, MgTPP showed 2 ± 1 ppm ferromagnetic impurity attributed to iron present in the magnesium source. MgT(3,4,5-OMe)PP could not be sublimed without decomposition and showed 5 ± 1 ppm ferromagnetic impurity as made. This impurity was carried along to the final product and corrected for in the magnetic data workup. The solvent content of each sample was measured by TGA postmagnetic experimentation to determine molecular mass used in magnetic data calculations. Infrared spectra (600−4000 ± 2 cm^{-1}) were obtained on a Bio-Rad FT-40 spectrophotometer as potassium bromide pellets. Fast atom bombardment (FAB) and liquid secondary ion mass spectrometry (LSIMS) were performed on a Finnigan MAT 95 mass spectrometer. The sample was first dissolved in CH_2Cl_2 and then added to a 3-nitrobenzyl alcohol matrix on the probe and bombarded by high-energy Cs^+ ions.

X-ray Structure Determination. Single crystals of **1a**, **1b**, and **2** were grown from their respective solvents and their unit cells determined on a Nonius KappaCCD diffractometer equipped with Mo Kα radiation ($\lambda = 0.71073$ Å). The crystallographic data are summarized in Table 2. Equivalent reflections were merged, and only those for which $I_o > 2\sigma(I)$ were included in the refinement, where $\sigma(F_o)^2$ is the standard deviation based on counting statistics. Reflections were indexed, integrated and corrected for Lorentz, polarization and absorption effects using DENZO-SMN and SCALEPAC.[19] The structure was solved by a combination of direct methods and heavy atom using SIR 97.[20] All of the non-hydrogen atoms were refined with anisotropic displacement coefficients. Hydrogen atoms were assigned isotropic displacement coefficients $U(H) = 1.2U(C)$ or $1.5U(C_{methyl})$, and their coordinates were allowed to ride on their respective carbons using SHELXL97.[21]

The final cycle of full-matrix least-squares refinement of **1a** was based on 4208 observed reflections [$I_o > 2\sigma(I)$] and converged with unweighted and weighted agreement factors $R(F) = 0.0548$ and $wR(F^2) = 0.1138$, respectively. There is one C_2 rotationally disordered solvent molecule of toluene in the unit cell.

(17) Brandon, E. J.; Rittenberg, D. K.; Arif, A. M.; Miller, J. S. *Inorg. Chem.* **1998**, *37*, 3376.
(18) Zegarac, S.; Napijalo, M. L.; Napijalo, M. M.; Nikolic, Z. *Fizika* **1976**, *8*, Supplement 159. Miller, J. S.; Krusic, P. J.; Dixon, D. A.; Reiff, W. M.; Zhang, J. H.; Anderson, E. C.; Epstein, A. J. *J. Am. Chem. Soc.* **1986**, *108*, 4459.
(19) Otwinowski, Z.; Minor, W. *Methods Enzymol.* **1997**, *276*, 307.
(20) Altomare, A.; Burla, M. C.; Camalli, M.; Cascarano, G.; Giacovazzo, C.; Guagliardi, A.; Moliteni, A. G. G.; Polidori, G.; Spagna, R. *SIR97—A program for automatic solution and refinement of crystal structure*, release 1.02. *J. Appl. Crystallogr.* **1999**, *32*, 115.
(21) Sheldrick, G. M. *SHELX97 [Includes SHELXS97, SHELXL97, CIFTAB]—Programs for Crystal Structure Analysis*, release 97-2); University of Göttingen: Göttingen Germany, 1997.

Table 2. Summary of the Crystallographic Data for [Mg(por•)][TCNQF$_4$]·*x*S

	[MgTPP][TCNQF$_4$]· PhMe, **1a**	[MgTPP][TCNQF$_4$] · 3(1,2-C$_6$H$_4$Cl$_2$), **1b**	[MgT(3,4,5-OMe)PP][TCNQF$_4$]· 3(1,2-C$_6$H$_4$Cl$_2$), **2**	MnT(3,4,5-OMe)PP][TCNQF$_4$]· 3(1,2-C$_6$H$_4$Cl$_2$)[24]
formula	$C_{63}H_{36}F_4MgN_8$	$C_{74}H_{40}Cl_6F_4MgN_8$	$C_{86}H_{64}Cl_6F_4MgN_8O_{12}$	$C_{86}H_{64}Cl_6F_4MnN_8O_{12}$
fw	1005.31	1355.16	1714.46	1745.09
space group	$P\bar{1}$	*C*2/*c*	*C*2/*c*	*C*2/*c*
a, Å	8.6151(3)	23.176(4)	16.9524(8)	16.9486(10)
b, Å	12.4746(6)	13.362(3)	25.8785(12)	25.7170(14)
c, Å	13.0295(6)	21.240(4)	19.3290(9)	19.4009(12)
α, deg	65.4109(18)	90	90	90
β, deg	78.103(3)	100.336(31)	106.507(2)	107.091(4)
γ, deg	80.565(3)	90	90	90
Z	1	4	4	4
V, Å^3	1241.13(9)	6470.8(3)	8130.2(7)	8082.8(8)
μ, cm^{-1}	1.03	3.38	2.96	4.39
ρ_{calcd}, g/cm^3	1.345	1.391	1.401	1.434
$R(F)^a$	0.0548	0.0538	0.0649	0.0547
wR(F^2)^b	0.1138	0.1233	0.1354	0.1340
T, K	200(1)	200(2)	200(1)	200(1)
λ, Å	0.71073	0.71073	0.71073	0.71073

^{a} $R(F) = \sum(|F_o| - |F_c|)/\sum|F_o|$. ^{b} $wR(F^2) = [\sum(w(F_o^2 - F_c^2)^2)/\sum(F_o^2)^2]^{1/2}$.

The final cycle of full-matrix least-squares refinement of **1b** was based on 3881 observed reflections [$I_o > 2\sigma(I)$] and converged with unweighted and weighted agreement factors $R(F) = 0.0538$ and wR(F^2) = 0.1233, respectively. The cations lie on crystallographic inversion centers with Mg at the center. There are three 1,2-dichlorobenzenes per magnesium in the asymmetric unit that are disordered by 180° rotation around one Cl−C bond.

The final cycle of full-matrix least-squares refinement of **2** was based on 4155 observed reflections [$I_o > 2\sigma(I)$] and converged with unweighted and weighted agreement factors $R(F) = 0.0649$ and wR(F^2) = 0.1354, respectively. The cations lie on crystallographic inversion centers with Mg at the center. There are three 1,2-dichlorobenzenes per magnesium in the asymmetric unit that are disordered by 180° rotation around one Cl−C bond.

X-ray CIF files for [MgTPP][TCNQF$_4$]·*x*S [S = PhMe, **1a**, (*x* = 1); S = 1,2-C$_6$H$_4$Cl$_2$, **1b**, (*x* = 3)] and [MgT(3,4,5-OMe)PP][TCNQF$_4$]·3(1,2-C$_6$H$_4$Cl$_2$) (**2**) have been deposited with the Cambridge Crystallographic Data Center, ref nos. CCDC-190229, CCDC-190231, and CCDC 190230, respectively.

Results and Discussion

Synthesis. Typical of manganoporphyrins, tetraarylporphinatomagnesium(II) reacts with strong electron acceptors in a variety of solvents. Common electron acceptors that are capable of oxidizing the porphyrin ring on Mg^{II}TPP ($E^\circ_{1/2}$ = 0.54 V in MeCN vs SCE)[11] are limited to TCNQF$_4$ and C$_4$(CN)$_6$, Table 1.

[MgTPP][TCNQF$_4$]·*x*S [S = PhMe, **1a** (*x* = 1); S = 1,2-C$_6$H$_4$Cl$_2$, **1b** (*x* = 3)], [MgT(3,4,5,-OMe)PP][TCNQF$_4$]·3(1,2-C$_6$H$_4$Cl$_2$) (**2**), [MgTPP][C$_4$(CN)$_6$]·*x*PhMe (**3**), and [MgT-(3,4,5,-OMe)PP][C$_4$(CN)$_6$]·*x*(1,2-C$_6$H$_4$Cl$_2$) (**4**) were isolated from the reaction of stoichiometric amounts of Mg^{II}(por) [H$_2$por = H$_2$TPP, H$_2$T(3,4,5-OMe)PP] and TCNQF$_4$ or C$_4$(CN)$_6$, with each being dissolved upon refluxing in the appropriate solvent (S) and filtered prior to reaction. The products appeared as shiny dark purple needles, plates, or powders. X-ray quality crystals were grown from solutions approximately 10% as concentrated or from solutions of 9:1 CH$_2$Cl$_2$/S. As occurs for [Mn(por)][TCNE]·*x*S, [Mg(por)][Z] (Z = TCNQF$_4$, C$_4$(CN)$_6$) incorporates aromatic solvents over aliphatic solvents, and hence, the aromatic solvate was isolated.[3a] Likewise, the solvent content varies with each structure, and the values reported herein are determined by X-ray structure analysis when all solvent sites are occupied. X-ray structure analyses for **3** and **4** were not possible due to very thin needlelike crystals isolated despite several attempts at various methods to maximize crystal growth. In this case, the solvent content was determined from TGA and elemental analyses. The solvent content of **1a**, **1b**, and **2** may be less than that determined crystallographically, and the actual solvent (*x*) content of magnetically characterized materials was determined by TGA and/or elemental analyses. Compound **3** differs from the other compounds as it exhibits rapid solvent loss at room temperature. Due to solvent loss of **3**, the accuracy of the elemental analysis is suspect. Therefore, the integrity of the molecular composition was also studied by mass spectroscopy.

Evidence of the formation of both the *π*-cation radical, [Mg^{II}(por•)]$^+$, and the reduced electron acceptor can be seen in the IR spectra by the disappearance of the sharp peak at 1009 cm^{-1} upon *π*-cation radical formation, for the donor. Both organic electron acceptors can undergo reversible one or two electron reductions.[12] While the cyano groups of [TCNQF$_4$]$^{\bullet-}$ are all equivalent, [C$_4$(CN)$_6$]$^{\bullet-}$ has three sets of equivalent cyano groups available for bonding. Table 3 provides a summary of ν_{CN} absorption for each of the acceptors as a function of coordination mode. The IR spectra for **1**−**4** clearly show a shift in ν_{CN} consistent with one electron reduction of TCNQF$_4$ and C$_4$(CN)$_6$. Upon reduction, ν_{CN} absrorptions occur at 2199 (s) and 2177 (m) cm^{-1}, **1a**, and 2212 (s) and 2187 (m) cm^{-1}, **1b**. These values are inconsistent with the ν_{CN} of TCNQF$_4^0$ [2225 (s sh) cm^{-1}]. Although the data are consistent with the values associated with the [TCNQF$_4$]$_2^{2-}$ dimer,[22a,23,24] the crystal structure for **1a** and **1b** clearly indicate *μ*-[TCNQF$_4$]$^{\bullet-}$ is present. The IR spectra for **3** and **4** show ν_{CN} values of 2210 (m) and 2185 (s), and 2218 (m) and 2183 (s) cm^{-1}, respectively. These values are inconsistent with C$_4$(CN)$_6^0$, 2247 (w), 2238 (m), and 2211(s) cm^{-1},[25] and indicate a 1-D chain structure similar to that of the manganese analogues with interior 2,3-*trans*-

Table 3. Summary of ν_{CN} for Various Configurations of $[TCNQF_4]^n$, $[C_4(CN)_6]^n$, and **1**−**4**

compd	ν_{CN}, cm^{-1}	ref
$TCNQF_4^0$	2225 (s)	22a, 23
$[TCNQF_4]^{2-}$	2168 (s), 2133 (m)	22a
$[TCNQF_4]_2^{2-}$	2195 (s), 2177 (m)	22a, 23
π-$[TCNQF_4]^{\bullet-}$	2194, 2172	44
μ-$[TCNQF_4]^{\bullet-}$	2196 (s), 2165 (m)	24
π-$C_4(CN)_6^o$	2247(w), 2238(m), 2211(s)	25
π-$[C_4(CN)_6]^{\bullet-}$	2185(s), 2168(m)	45
trans-1,4-$[C_4(CN)_6]^{\bullet-}$	2193(s), 2150(s)	41
trans-2,3-$[C_4(CN)_6]^{\bullet-}$	2217(m), 2190(m)	27j
π-$[C_4(CN)_6]_2^{2-}$	2185(s), 2170(m), 2128(m)	27j
π-$[C_4(CN)_6]^{2-}$	2200(m), 2152(s), 2124(w)	46
π-*iso*-$[C_4(CN)_6]^{2-}$	2174(s), 2158(m)	46
trans−1,4-$[C_4(CN)_6]^{2-}$	2181(vs), 2107(sh), 2141(s), 2130(sh)	41
$[C_4(CN)_5O]^-$	2235(w sh), 2226(m), 2218(s), 1557(m)	46
1a	2199 (s), 2177 (m)	*b*
1b	2212 (s), 2187 (m)	*b*
2	2194 (s), 2172 (m)	*b*
3	2210 (m), 2185 (s)	*b*
4	2218 (m), 2183 (s)	*b*

[a] Seen only in the solvated material. [b] This work.

μ-N-σ-binding. The IR spectra do not change upon heating and desolvation of the samples to 200 °C in Nujol mulls.

Structure. The structures of **1a**, **1b**, and **2** were determined by single crystal X-ray analyses. The unit cell and metric parameters are summarized in Table 2, and the ORTEP drawings are presented in Figures 1−3. In each case, the structures of the $[Mg^{II}(por^{\bullet})]^+$ cations, which lie on crystallographic inversion centers at Mg, are nearly indistinguishable and consistent with other related $[Mg^{II}(por^{\bullet})]^+$ and $[Mn^{III}(por)]^+$ cations reported in the literature.[26,27] The $por^{\bullet+}$ species is planar with Mg−N(pyrrole) bond distances averaging 2.071 ± 0.012 Å. This distance is comparable to that found in other six-coordinate Mg porphyrins such as $Mg^{II}TPP(L)_2$ (L = 1-methylimidazole, 4-picoline, and piperidine)[26a] (2.075 ± 0.007 Å) but is shorter than the five-coordinate $[Mg^{II}(TPP^{\bullet})]^+[ClO_4]^-$ (2.096 Å),[28] due to the out-of-plane displacement of Mg. The Mg−N(pyrrole) bond distances are longer than the 2.01 Å average for Mn−N(pyrrole) due to the larger ionic radii of Mg(II) compared to Mn(II).[29] The bond distances and angles of the porphyrin ring are identical within the limits of the standard deviation between $[Mg^{II}(por^{\bullet})]^+$, $Mg^{II}(por)$, $[Mn^{III}(por)]^+$, and $[Mn^{II}(por)]$.

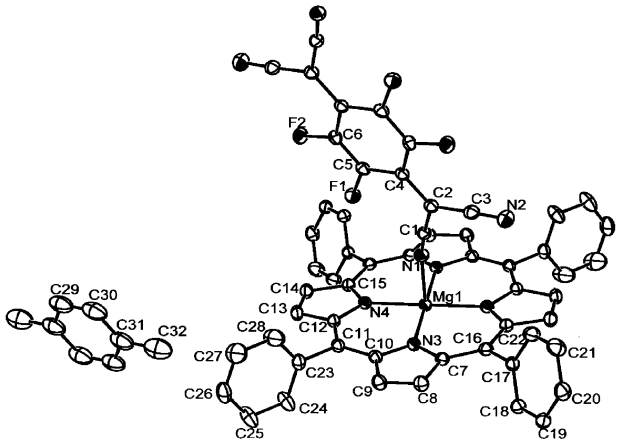

Figure 1. ORTEP labeling diagram (30%) of [MgTPP][TCNQF$_4$]·PhMe, **1a**.

The $TCNQF_4$ is essentially planar with a small deviation of the dicyanomethylene twisted from the benzenoid ring plane by ∼5°. The C_F-C_F, C_F-C_C, and C_C-C_{CN} distances

(22) (a) Sugimoto, T.; Ueda, K.; Tsujii, M.; Fujita, H.; Hosoito, N.; Kanehisa, N.; Shibamoto, Y.; Kai, Y. *Chem. Phys. Lett.* **1996**, *249*, 304. (b) Hotta, S.; Kobayashi, H. *Synth. Met.* **1994**, *66*, 117. (c) Sugano, T.; Hashida, T.; Kobayashi, A.; Kobayashi, H.; Kinoshita, M. *Bull. Chem. Soc. Jpn.* **1988**, *61*, 1, 2303. (d) Hoshino-Miyajima, N.; Luneau, I.; Mitani, T.; Maruyama, Y. *Bull. Chem. Soc. Jpn.* **1994**, *67*, 622. (e) Friederichs, S.; Kudnig, J.; Klar, G. *Z. Naturforsch., B: Chem. Sci.* **1996**, *51*, 1295. (f) Stein, D.; Sitzmann, H.; Boese, R.; Dormann, E.; Winter, H. *J. Organomet. Chem.* **1991**, *412*, 143. (g) Fourmigué, M.; Domereq, B.; Jourdain, I.; Molinie, P.; Guyon, F.; Amaudrut, J. *Chem. Eur. J.* **1998**, *4*, 1714. (h) Fourmigué, M.; Perrocheau, V.; Clerac, R.; Coulon, C. *J. Mater. Chem.* **1997**, *7*, 2235. (i) Soos, Z. G.; Keller, H. J.; Ludolf, K.; Queckborner, J.; Wehe, D.; Flandrois, S. *J. Chem. Phys*, **1981**, *76*, 5287. (j) Nakatsuji, S.; Takai, A.; Nishikawa, K.; Morimoto, Y.; Yasuoka, N.; Suzuki, K.; Enoki, T.; Anzai, H. *J. Chem. Soc., Chem. Commun.* **1997**, *182*, 275. (k) Emge, T. J.; Bryden, W. A.; Wiygul, F. M.; Cowen, D. O.; Kistenmacher, T. J. *J. Chem. Phys*. **1982**, *77*, 3188. (l) Emge, T. J.; Cowen, D. O.; Bloch, A. N.; Kistenmacher, T. J. *Mol. Cryst. Liq. Cryst.* **1983**, *95*, 191. (m) Wygul, F. M.; Emge, T. J.; Kistenmacher, T. J. *Mol. Cryst. Liq. Cryst.* **1982**, *90* 163.

(23) Dixon, D. A.; Calabrese, J. C.; Miller, J. S. *J. Phys. Chem*. **1988**, *93*, 2284.

(24) Johnson, M. T.; Arif, A. M.; Miller, J. S. *Eur. J. Inorg. Chem*. **2000**, 1781.

(25) Dixon, D. A.; Calabrese, J. C.; Miller, J. S. *J. Phys. Chem*. **1991**, *95*, 3139; *J. Phys. Chem*. **1991**, *95*, 7960.

(26) (a) McKee, V.; Ong, C. C.; Rodley, G. A. *Inorg. Chem*. **1984**, *23*, 4242. (b) Barkigia, K. M.; Spaulding, L. D.; Fajer, J. *Inorg. Chem*. **1983**, *22*, 349.

(27) (a) Hibbs, W.; Rittenberg, D. K.; Sugiura, K.-i.; Burkhart, B. M.; Morin, B. G.; Arif, A. M.; Liable-Sands, L.; Rheingold, A. L.; Sundaralingam, M.; Epstein, A. J.; Miller, J. S. *Inorg. Chem.* **2001**, *40*, 1915. (b) Miller, J. S.; Epstein, A. J. *Chem. Commun.* **1998**, 1319. (c) Goldberg, I.; Krupitsky, H.; Stein, Z.; Hsiou, Y.; Strouse, C. E. *Supramol. Chem* **1995**, *4*, 203. (d) Krupitsky, H.; Stein, Z.; Goldberg, I. *J. Inclusion Phenom. Mol. Recognit. Chem.* **1995**, *20*, 211. (e) Goldberg, I. *Mol. Cryst. Liq. Cryst*. **1996**, *278*, 767. (f) Byrn, M. P.; Curtis, C. J.; Hsiou, Y.; Kahn, S. I.; Sawin, P. A.; Tendick, S. K.; Terzis, A.; Strouse, C. E. *J. Am. Chem. Soc*. **1993**, *115*, 9480. (g) Rittenberg, D. K.; Sugiura, K.-i.; Sakata, Y.; Mikami, S.; Epstein, A. J.; Miller, J. S. *Adv. Mater*. **2000**, *12*, 126. (h) Rittenberg, D. K.; Sugiura, K.-i.; Sakata, Y.; Guzei, I. A.; Rheingold, A. L.; Miller, J. S. *Chem. Eur. J.* **1999**, *5*, 1874. (i) Böhm, A.; Vazquez, C.; McLean, R. S.; Calabrese, J. C.; Kalm, S. E.; Manson, J. L.; Epstein, A. J.; Miller, J. S. *Inorg. Chem.* **1996**, *35*, 3083. (j) Sugiura, K.-i.; Arif, A.; Rittenberg, D. K.; Schweizer, J.; Öhrstrom, L.; Epstein, A. J.; Miller, J. S. *Chem. Eur. J.* **1997**, *3*, 138. (k) Brandon, E. J.; Sugiura, K.-i.; Arif, A. M.; Liable-Sands, A.; Rheingold, A. L.; Miller, J. S.; *Mol. Cryst. Liq. Cryst.* **1997**, *305*, 269. (l) Brandon, E. J.; Burkhart, B. M.; Rogers, R. D.; Miller, J. S. *Chem. Eur. J.* **1998**, *4*, 1938. (m) Brandon, E. J.; Arif, A. M.; Burkhart, B. M.; Miller, J. S. *Inorg. Chem.* **1998**, *37*, 2792. (n) Brandon, E. J.; Arif, A. M.; Miller, J. S.; Sugiura, K.-i.; Burkhart, B. M. *Cryst Eng*. **1998**, *1*, 97. (o) Sugiura, K.-i.; Mikami, S.; Tanaka, T.; Sawada, M.; Manson, J. L.; Miller, J. S.; Sakata, Y. *Chem. Lett.* **1997**, 1071. (p) Day, V. W.; Sults, B. R.; Tasset, E. L.; Marianelli, R. S.; Boucher, L. J. *Inorg. Nucl. Chem. Lett*. **1975**, *11*, 505. (q) Cheng, B.; Cukiernik, F.; Fries, P.; Marchon, J.-C.; Scheidt, W. R. *Inorg. Chem.* **1995**, *34*, 4627. (r) Guildard, R.; Perie, K.; Barbe, J.-M.; Nurco, D. J.; Smith, K. M.; Caemelbecke, E. V.; Kadish, K. M. *Inorg. Chem.* **1998**, *37*, 973. (s) Landrum, J. T.; Hatano, K.; Scheidt, W. R.; Reed, C. A. *J. Am. Chem. Soc.* **1980**, *102*, 6729. (t) Hill, C. L.; Williamson, M. M. *Inorg. Chem.* **1985**, *24*, 3024. (u) Fleischer, E. B. *Acc. Chem Res.* **1970**, *3*, 105. (v) Scheidt, W. R.; Reed, C. A. *Chem. Rev.* **1981**, *81*, 543. (w) Turner, P.; Gunter, M. J.; Hambley, T. W.; White, A. H.; Skelton, B. W. *Inorg. Chem.* **1992**, *31*, 2297.

(28) Brancato-Buentello, K.; Scheidt, W. R. *Angew. Chem., Int. Ed. Engl*. **1997**, *36*, 1456.

(29) *Lang's Handbook of Chemistry*, 11th ed.; Dean, J. A, Ed.; McGraw-Hill: New York, 1973; pp 3−120.

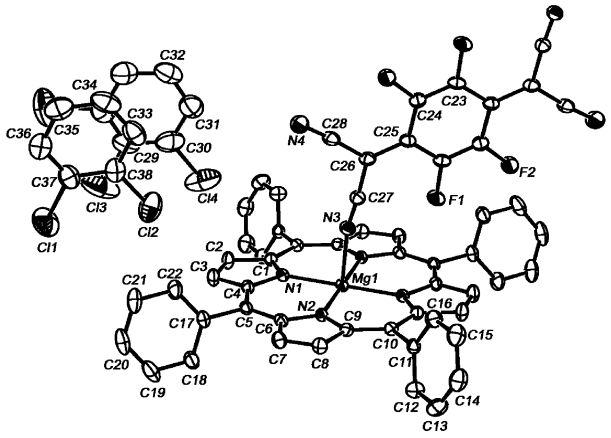

Figure 2. ORTEP labeling diagram (30%) of [MgTPP][$TCNQF_4$]·3(1,2-$C_6H_4Cl_2$), **1b**.

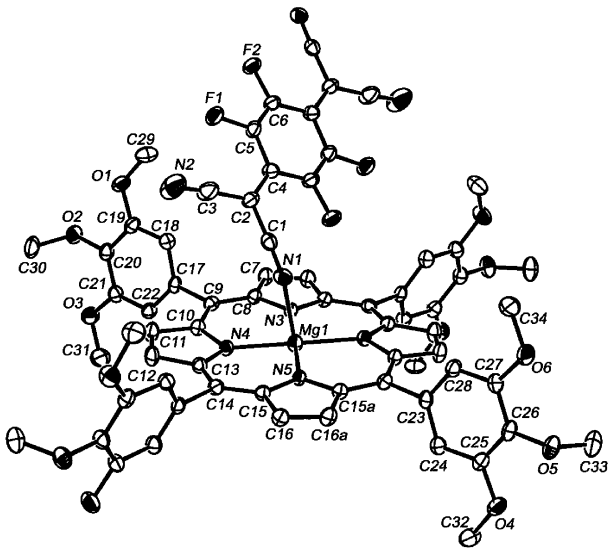

Figure 3. ORTEP labeling diagram (30%) of [MgT(3,4,5-OMe)PP][$TCNQF_4$]·3(1,2-$C_6H_4Cl_2$), **2**. Solvents have been omitted for clarity.

range from 1.337(5) to 1.355(4), 1.412(4) to 1.421(5), and 1.403(5) to 1.416(2) Å, respectively, which differ from those of $TCNQF_4$[0] [22,30] but are comparable to the values for reduced $TCNQF_4$ as either $[TCNQF_4]_2^{2-}$ [12,22,23] or μ-$[TCNQF_4]^{\bullet-}$,[23] as observed from the IR data. The C−C(CN)$_2$ distance best describes the oxidation state of $[TCNQF_4]^n$ as this bond increases as the negative charge increases for $[TCNQF_4]^n$. The C−CN bonds average 1.348 Å, consistent with the formulation of $TCNQF_4$ as $[TCNQF_4]^{\bullet-}$ [23] as observed from the IR data. $[TCNQF_4]^{\bullet-}$ is uniformly *trans*-μ-N-σ-bound to two Mg's, forming 1-D parallel chains of alternating $S = {}^1/_2$ cations and $S = {}^1/_2$ anions in a $\cdots D^{\bullet+}A^{\bullet-}D^{\bullet+}A^{\bullet-}\cdots$ (D = Mg(por$^\bullet$); A = $TCNQF_4$) motif (Figures 4−6) as noted for the Mn analogues with $TCNQF_4$[24] and TCNE.[3a,7a,8]

The $[TCNQF_4]^{\bullet-}$−N−Mg distances range from 2.221(2) to 2.276(3) Å, and $MgNC_{TCNF_4}$ angles range from 141.3(2)° to 167.8 (2)°. The dihedral angle between the mean MgN_4 and the mean $[TCNQF_4]^{\bullet-}$ planes range from 46.6° to 89.5°.

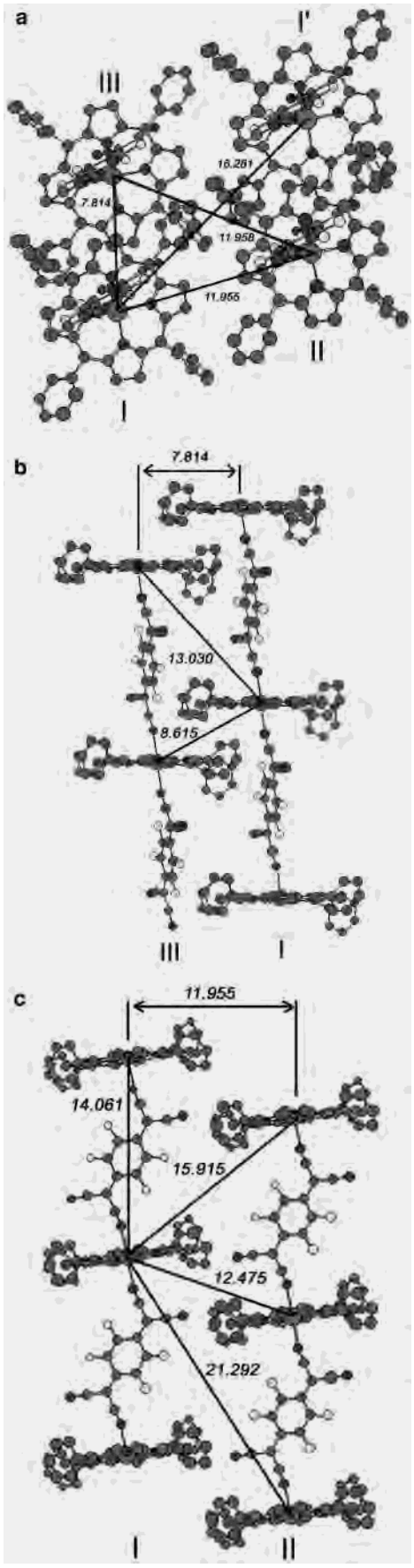

Figure 4. View down the *a*-axis normal to the parallel chains showing the interchain interactions between chains **I**, **II**, and **III** (a). View parallel to chains **I** and **III** (b) and **I** and **II** (c) for [MgTPP][$TCNQF_4$]·PhMe, **1a**.

(30) Emge, T.; Maxfield, M.; Cowan, D.; Kistenmacher, T. J. *Mol. Cryst. Liq. Cryst.* **1981**, *65*, 161.

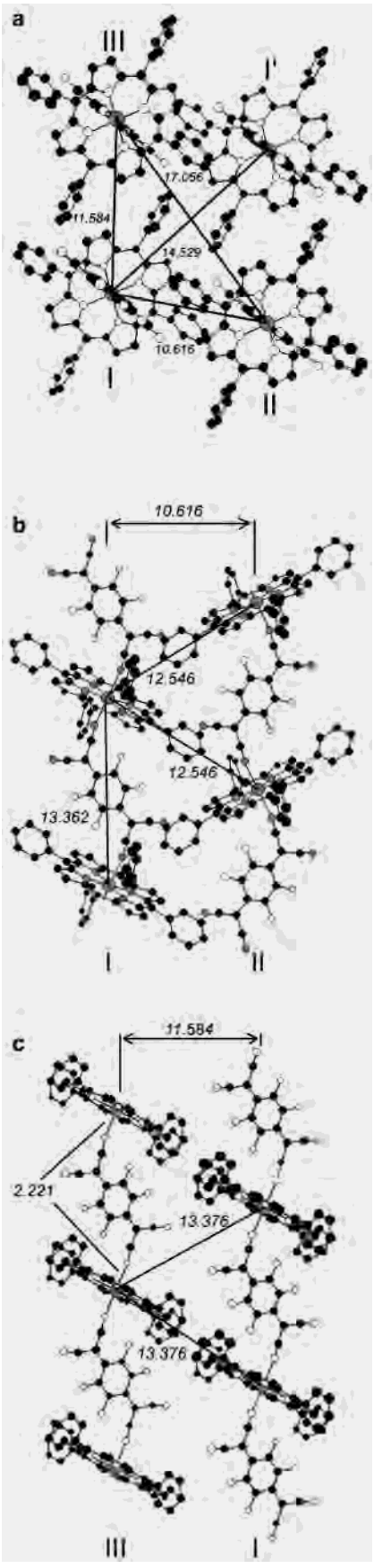

Figure 5. View down the *a*-axis normal to the parallel chains showing the interchain interactions between chains **I**, **II**, and **III** (a). View parallel to chains **I** and **II** showing herringbone arrangement of porphyrins (b) and **I** and **III** (c) for [MgTPP][TCNQF$_4$]·3(1,2-$C_6H_4Cl_2$),**1b**.

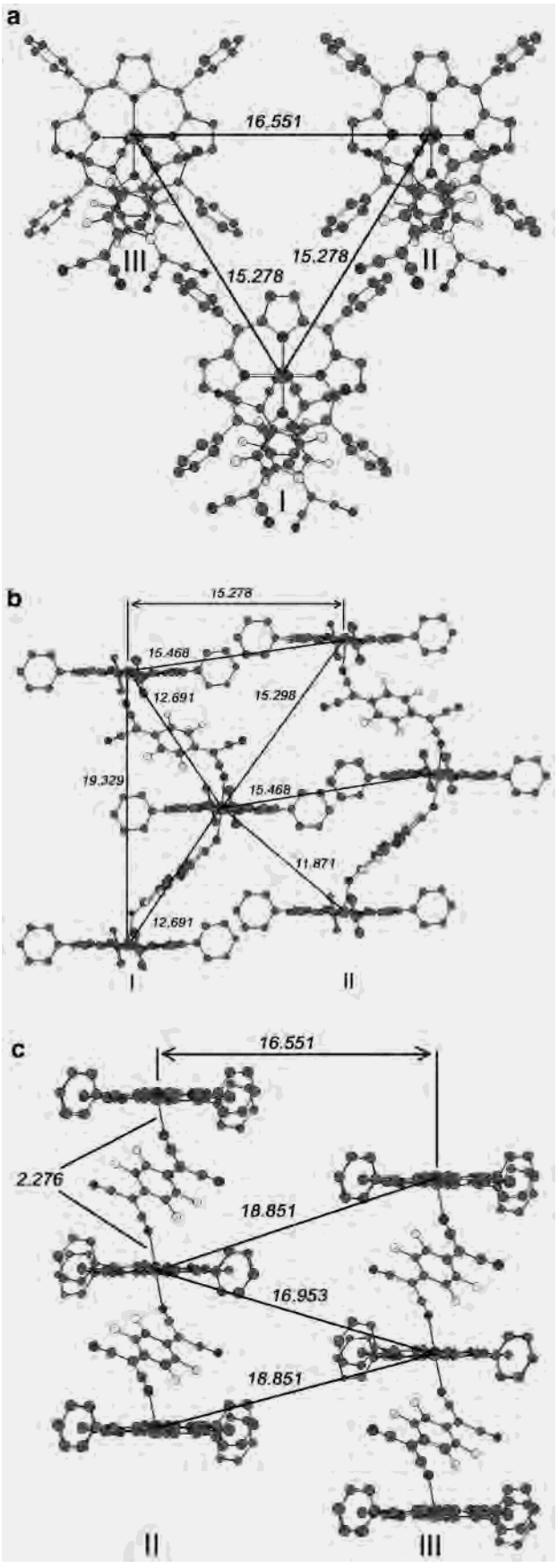

Figure 6. View down the *a*-axis normal to the parallel chains showing the interchain interactions between chains **I**, **II**, and **III** (a). View parallel to chains **I** and **II** showing the zigzag configuration along the chain (b) and **II** and **III** (c) for [MgT(3,4,5-OMe)PP][TCNQF$_4$]·3(1,2-$C_6H_4Cl_2$), **2**.

Table 4. Summary of Key Bond Distances and Separations for [Mg(por•)][$TCNQF_4$]·*x*S

compd	[MgTPP][$TCNQF_4$]· PhMe, **1a**	[MgTPP][$TCNQF_4$]· 3(1,2-$C_6H_4Cl_2$), **1b**	[MgT(3,4,5-OMe)PP][$TCNQF_4$]· 3(1,2-$C_6H_4Cl_2$), **2**	[MnT(3,4,5-OMe)PP][$TCNQF_4$]· 3(1,2-$C_6H_4Cl_2$)[24]
MN_{CN}, Å	2.2661(16)	2.221(2)	2.276(3)	2.321(3)
MNC, deg	167.83(15)	167.5(2)	141.3(3)	135.9(2)
dihedral angle, deg	84.5	89.5	46.6	46.4
MN_{por}, Å	2.0716(14)	2.0681(19)	2.081(4)	1.998(2)
	2.0742(15)	2.079(2)	2.064(4)	2.002(3)
			2.059(3)	2.013(3)
$N_{por}-M-N_{CN}$, deg	94.34(6)	90.17(8)	96.42(11)	91.69(7)
	93.07(6)	93.21(8)	92.70(9)	95.72(10)
			87.30(9)	88.31(7)
				84.27(10)
$N_{CN}-M-N_{CN}$,*o*	180	180(14)	174.60(17)	176.63(13)
M···M, Å intrachain	14.061	13.362	12.691	12.685
Mg···Mg, Å interchain	13.030	12.546	15.468	15.400
	8.615	13.376	15.298	15.368
	15.915		11.871	11.812
	12.475		18.851	18.749
			16.953	16.949
interchain separation, Å	7.814	11.584	15.278	15.197
	11.955	10.616	16.551	15.199
	11.958	14.529		16.515
	16.281	17.056		

These values are typical of related compounds.[24,27] The intrachain Mg···Mg separations range from 12.691 to 14.061 Å.

Although not isomorphous, **1a** is structurally similar to previously reported [MnTPP][TCNE] compounds.[8,27] Compounds **1b** and **2** also belong to the *C*2/*c* space group, and **2** is isomorphous to [MnT(3,4,5-OMe)PP][$TCNQF_4$]·3(1,2-$C_6H_4Cl_2$).[24] Compounds **1a**, **1b**, and **2** form parallel 1-D chains with the key inter- and intrachain separations noted in Table 4 and Figures 4−6.

Compound **1a** forms identical 1-D chains with an average nearest-neighbor interchain separation of 12.017 Å, approximately 10% more compact than its Mn(III) analogue. When the metal centers of the chain are aligned along a vertical axis, the porphyrins are tilted in a uniform direction and the $TCNQF_4$ plane forms a 84.5° dihedral angle with the plane of the porphyrin (Figure 4b). The largest reported dihedral angle for an unsubstituted [MnTPP][TCNE] is 82.3°, in the case of the *o*-xylene solvate.[27a]

The presence of a mirror plane between two porphyrin chains in the unit cell of **1b** results in a herringbone arrangement of chains (Figure 5). This configuration is also exhibited in [MnTPP][TCNE]·2(1,3-$C_6H_4Cl_2$), which has similar interchain separations.[27a] Within the chain, the [$TCNQF_4$]$^{\bullet-}$ plane forms an 89.5° dihedral angle to the mean plane of the porphyrin and is the largest dihedral observed for this family of materials. This is in contrast with one of the smallest reported angles of 29.9° for [MnTPP][TCNE]·2(1,3-$C_6H_4Cl_2$).[27a] Therefore, the porphyrins along the chain in Mg have less tilt than those along the Mn chain resulting in much greater Mg···Mg intrachain separations.

Compound **2** is the second example with parallel chains possessing a zigzag motif as a result of the [$TCNQF_4$]$^{\bullet-}$ species aligning *cis* with respect to each other about the metal center (Figure 6b). The only other report of this zigzag pattern is for the manganese analogue for this compound.[24] In these cases, every other porphyrin along the chain is eclipsed, and the chain appears to form in two columns. The unit cell dimensions and the M···M (M = Mg, Mn) intra- and interchain distances vary by less than 1%. Additionally, similar dihedral angles between the [$TCNQF_4$]$^{\bullet-}$ plane and the [MT(3,4,5-OMe)PP]$^+$ plane are nearly identical at 46.4° and 46.6° for M = Mn(III) and Mg(II), respectively.

For **1a**, **1b**, and **2**, the porphyrin groups of neighboring chains are offset such that Mg···Mg interchain separations are different from the general interchain separation, Figures 4−6. Key bond distances and angles are listed in Table 4. In summary, Mg···Mg intrachain separations range from 12.691 (**2**) to 14.061 (**1a**) Å which are larger than the typical M···M separation for [TCNE]$^{\bullet-}$ compounds (i.e., 8.587 to 10.376 Å) in order to accommodate the larger [$TCNQF_4$]$^{\bullet-}$, but **2** and its Mn analogue are identical. In contrast, the interchain separations are comparable and range from 7.814 (**1a**) to 17.056 (**1b**) Å. The $Mg-N_{CN}$ distances are 2.266, 2.221, and 2.276 Å, and the MgNC angles are 167.8°, 167.5°, and 141.3°, respectively, for **1a**, **1b**, and **2**. The C_2 disordered aromatic solvent molecules fill the voids in the structure. Attempt to determine the single crystal X-ray structure of the [$C_4(CN)_6$]$^{\bullet-}$ salts were unsuccessful due to the lack of suitable crystals.

Mass Spectroscopy. Compounds **2** and **3** were analyzed by mass spectroscopy, which confirmed the presence of the parent cation with a peak at 636.2 and 997.3 amu, respectively. With no crystal structure available, the results of the mass spectroscopy for **3** verify that no chemistry has occurred on the periphery of the porphyrin ring. Due to the high molecular weight and ionic nature of the compound, FAB mass spectroscopy was utilized since it does not require thermal vaporization of the sample. FAB does not readily cause degradation of the molecule; therefore, it is common to see only the peaks relevant to the parent cation. Compound **2**, however, did demonstrate four sets of peaks separated by 14 amu, consistent with the loss of four methyl groups, believed to originate from the *p*-methoxy groups on the porphyrin ring.

Magnetic Data. The 2−300 K corrected molar magnetic susceptibility, χ, was measured for **1**−**4**, and the data are

Chart 1

$$\chi = \frac{Ng^2\mu_B^2}{k_B(T-\theta)}\frac{0.25+0.14995x+0.30094x^2}{1+1.9862x+0.68854x^2+6.0626x^3} \qquad x=\frac{|J|}{k_BT} \qquad (1)$$

$$\chi = \frac{Ng^2\mu_B^2}{4k_B(T-\theta)}\left[\frac{1+0.57979916K+16.902653K^2+29.376885K^3+29.832959K^4+14.036918K^5}{1+2.7979916K+7.0086780K^2+8.6538644K^3+4.5743114K^4}\right]^{2/3} \qquad K=\frac{J}{2k_BT} \qquad (2)$$

$$\chi = \frac{Ng^2\mu_B^2}{k_B(T-\theta)}\frac{0.25+0.063465x+0.0140763x^2}{1+0.687355x+0.58384582x^2+0.179409x^3} \qquad x=\frac{2|J|}{k_BT} \quad \sigma=1 \qquad (3)$$

Table 5. Summary of Room Temperature Magnetic Moment, μ_B, Weiss Constant, θ, and Intrachain Coupling, J_{Intra}, for **1**−**4**

	μ_B (300 K), obsd[a]	θ, K	J_{intra}/k_B, K, Bonner−Fisher	J_{intra}/k_B, K, Pade	J_{intra}/k_B, K, Hatfield	J_{intra}/k_B, K, av
1a	2.28	−1.4	−3.1	−3.1	−2.9	−3.0 ± 0.1
1b	2.43	−1.4	−2.6	−2.6	−2.6	−2.6 ± <0.1
2	2.13	*b*	*b*	*b*	*b*	*b*
3	2.37	−0.57	−0.3	−1.3	−0.9	−0.8 ± 0.5
4	2.43	*b*	*b*	*b*	*b*	*b*

[a] Room-temperature moment calculated for two $S = {}^1/_2$ spins is 2.45 μ_B. [b] J values not reported for **2** and **4** due to unusually low magnetic moment; see text.

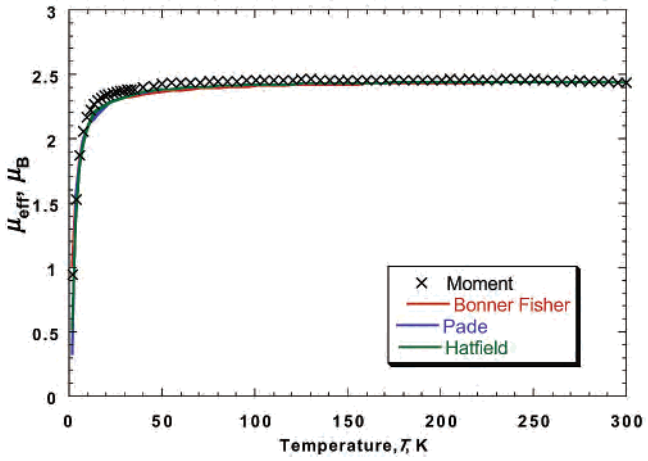

Figure 7. $\mu_{eff}(T)$ for **1b** normalized to the calculated moment of 2.45 μ_B and fit to the Bonner−Fisher (red), Pade (blue), and Hatfield (green) expressions with respective J_{intra}/k_B values of −2.6, −2.6, and −2.6 K.

summarized in Table 5. The 300 K effective moments, μ_{eff} [$\equiv(8\chi T)^{1/2}$], of **1a**, **1b**, and **3** are 2.28, 2.43, and 2.37 μ_B, respectively, averaging 2.36 μ_B, in accord with the expected value for two $S = {}^1/_2$ spins of 2.45 μ_B, with antiferromagnetic coupling.[31] In each case, the moment remains relatively constant with decreasing temperature until approximately 50−100 K (Figure 7). A rapid decrease occurs below 30 K, with the moment approaching zero as $T \rightarrow 0$ K, indicating antiferromagnetic interactions at low temperature. The $\mu(T)$ value can be fit to the Curie−Weiss expression, χ [$\propto 1/(T-\theta)$], with θ of −1.4, −1.4, and −0.57 K for **1a**, **1b**, and **3**, respectively, indicating weak antiferromagnetic coupling.

The [MnTPP][TCNE]·xS family of compounds has significant antiferromagnetic intrachain interactions and order as ferrimagnets. Typically, the $\mu(T)$ data above 50 K can be fit to the Seiden expression[32] for a uniform isolated 1-D chain composed of alternating quantum ($S = {}^1/_2$) and classical ($S = 2$) spin sites. However, below ∼50 K, the onset of long-range interchain coupling occurs, and no appropriate magnetic model exists. This magnetic behavior is also reported for [MnT(3,4,5-OMe)PP][TCNQF$_4$]·3(1,2-$C_6H_4Cl_2$).[24] This compound, even with its unique zigzag structural motif, has a critical temperature of 7.3 K, coercive field of 17.1 kOe, and intrachain coupling, J_{intra}/k_B, of −71 K,[33] based upon the Seiden model.

The Seiden model,[32] however, is not applicable for the [Mg^{II}(por$^{\bullet}$)]$^+$ materials reported herein as this model is for isolated chains of alternating quantum and classical spins, and both [Mg^{II}(por$^{\bullet}$)]$^+$ and the radical anion have $S = {}^1/_2$ quantum spins. Hence, due to the uniform chain structure, the intrachain 1-D coupling values, J_{intra}, of **1a**, **1b**, and **3** were determined from modeling $\mu(T)$ to three different, albeit similar, models, namely the Bonner−Fisher (BF),[34] Pade,[35] and Hatfield[36] models (Figure 7), eqs 1−3 (Chart 1), respectively, for uniform 1-D linear chains with $S = {}^1/_2$ spin sites[37] and a Landé value, $g = 2.003$, as measured by EPR.

The J_{intra}/k_B values of −3.0 ± 0.1, −2.6 ± <0.1, and −0.8 ± 0.5 K for **1a**, **1b**, and **3**, respectively, calculated by eqs 1−3, indicate weak antiferromagnetic intrachain coupling. The Bonner and Fisher model, eq 1, describes a Heisenberg system of antiferromagnetically coupled uniformly spaced spins. While eq 1 estimates the susceptibility from a single polynomial expression, eq 2 is derived from the ratio of two polynomials, allowing for a better approximation of the susceptibility. The Hatfield expression, eq 3, further extends the model to include systems of alternating coupling constants J and σJ with $\sigma = 1$, as **1a**, **1b**, and **3** form uniform linear chains. All three models are in good agreement and accurately model the magnetic behavior **1a**, **1b**, and **3**.

The antiferromagnetic coupling observed for **1a** and **1b** is attributed to the delocalized unpaired electron spin residing in the plane of the [Mg^{II}(por$^{\bullet}$)]$^+$ a_{2u} (π) SOMO[38] as noted for MnTPPs,[39] interacting with the delocalized spin residing

(31) Values less than the calculated spin only value of 2.45 μ_B are attributed to weighing errors due to errors in molecular weight due to the specific degree of solvation and subtraction of the ferromagnetic impurity.

(32) Seiden, J. *J. Phys., Lett.* **1983**, *44*, L947.
(33) $H = -2J\mathbf{S_a}\cdot\mathbf{S_b}$.
(34) Bonner, J. C.; Fisher, M. E. *Phys. Rev.* **1964**, *135*, A640.
(35) Baker, G. A.; Rushbrooke, G. S.; Gilbert, H. E. *Phys. Rev.* **1964**, *135*, A1272.
(36) Hall, J. W.; Marsh, W. E.; Weller, R. R.; Hatfield, W. E. *Inorg. Chem.* **1981**, *20*, 1033.
(37) Equations 1−3 calculate χ per spin; however, for linear chain compounds, χ is calculated per one donor−acceptor unit that contains two spin sites. As such, the results of eqs 1−3 are multiplied by two to represent the two spin unit.

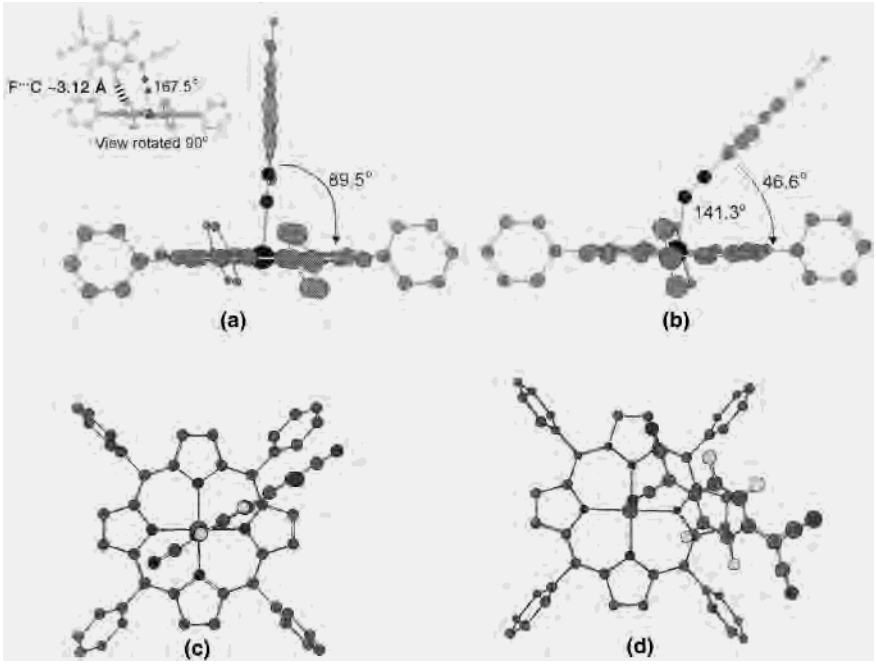

Figure 8. The MgNC angle (darker atoms) and dihedral angle between the mean μ-$[TCNQF_4]^{\bullet-}$ and porphyrin planes (shown with arrows) are (a) 167.5° and 89.5°, respectively, for **1b** and (b) 141.3° and 46.6°, respectively, for **2**. The nearest neighbor interactions for **1b** and **2** are illustrated in parts c and d, respectively.

in the plane of the $[TCNQF_4]^{\bullet-}$ a_g (π^*) SOMO.[23,40] Due to the 87 ± 2.5° dihedral angle between the mean $[TCNQF_4]^{\bullet-}$ and $[Mg^{II}(por^{\bullet})]^+$ planes for **1a** and **1b**, the closest contacts occur between a F and a 2-pyrrole carbon (F···C ~3.12 Å) (Figure 8a (inset), c) via a nonbonded electron pair on that F. This leads to weak antiferromagnetic coupling in accord with the estimated values of J_{intra}/k_B of $-2.8_5 \pm 0.2_5$ K for **1a** and **1b**. The stronger antiferromagnetic coupling reported for the $S = 2$ $[Mn^{III}por]^+$ family, e.g., −33 K for [MnTClPP]-[TCNE]·2PhMe [H_2TClPP = tetrakis(4-chlorophenyl)porphyrin] that has a similar dihedral angle of 86.8°,[17] is not attributed to this overlap as the unpaired spin is primarily localized on the Mn^{III}. Overlap occurs via the Mn^{III} d_{z^2} orbital and the π_z orbital of the N-bound nitrile of $[TCNQF_4]^{\bullet-}$, by analogy to $[TCNE]^{\bullet-}$ (Figure 9a), and the lower the MnNC angle the greater the overlap and the stronger the coupling as observed.[10]

In contrast, the $[MgT(3,4,5\text{-}OMe)PP]^+$-containing compounds, **2** and **4**, have substantially reduced magnetic susceptibility over the 2−300 K temperature range and are associated with noisy data sets arising from the extraction of these lower moments from large diamagnetic corrections, in part due to three 1,2-dichlorobenzene solvates and a bulky porphyrin containing 12 methoxy groups. By correcting for ppm-level ferromagnetic impurities (0−21 ppm), the overall shape and slope of the data from 2 to 300 K is reproducible for five unique data sets of **2**. In each case, the 5 K moment

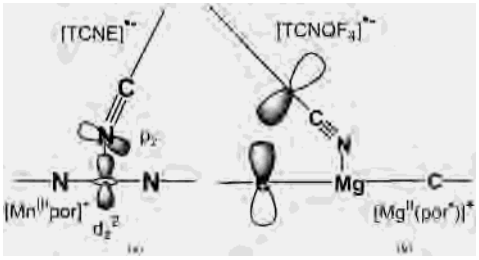

Figure 9. Comparison of the $d_{z^2}-p_z$ (of the π_z) orbital overlap between $[TCNE]^{\bullet-}$ *trans*-μ-N-σ-bound to $[Mn^{III}(por)]^+$ (a), and a p_z orbital of the delocalized SOMO π-orbitals of $[TCNQF_4]^{\bullet-}$ and $[Mg^{II}(por^{\bullet})]^+$ (b). The horizontal line represents the plane of the porphyrin between the unbound *meso*-C and Mg atoms.

is ~0.85 μ_B with a very slight turn toward zero below 5 K. Above 5 K, the moment increases linearly to 2.13 μ_B at room temperature. Similar reproducibility is observed for **4**, which has a 5 K moment of 1.30 μ_B and a very slight turn toward zero below 5 K. An increase in temperature shows a near linear increase of the moment of 2.43 μ_B. As a consequence of the very low moments, $\mu(T)$ could not be meaningfully fit to either the Curie−Weiss expression or any of the 1-D chain models, eqs 1−3. However, each model suggests stronger antiferromagnetic interactions with J_{intra}/k_B values approximately −85 and −60 K, **2** and **4**, respectively, based on the gradual increase in $\mu(T)$ with increasing temperature. However, the curvature of the modeled moments does not represent the observed linear increase, and there are significant deviations at low temperature as the observed moments are noticeably above zero at 2 K. In summary, the magnetic data for **2** and **4** cannot be reasonably fit to available models. Nonetheless, the reduced room-temperature moment and low values of $\mu(T)$ are attributed to significantly stronger antiferromagnetic coupling present for the $[MgT(3,4,5\text{-}OMe)PP]^+$ compounds, **2** and **4**, with respect to **1a** and **1b**.

(38) Barzilay, C, M.; Sibilia, A. A.; Spiro, T. G.; Gross, Z. *Chem. Eur. J.* **1995**, *1*, 222. Turner, P.; Gunter, M. J. *Inorg. Chem.* **1994**, *33*, 1406. Gasyna, Z.; Stillman, M. J. *Inorg. Chem.* **1990**, *29*, 5101. Fajer, J.; Borg, D. C.; Forman, A.; Felton, R. H.; Vegh, L.; Dolphin, D. *Ann. N. Y. Acad. Sci.* **1973**, *206*, 349.
(39) Mishra, S.; Chang, J. C.; Das, T. P. *J. Am. Chem. Soc.* **1980**, *102*, 2674.
(40) Brocks, G. *Phys. Rev. B: Condens. Matter* **1997**, *55*, 6816.

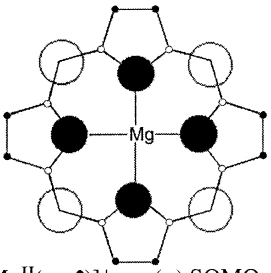

$[Mg^{II}(por^{\bullet})]^+$ a_{2u} (π) SOMO

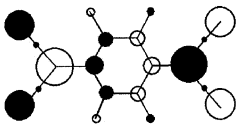

$[TCNQF_4]^{\bullet-}$ a_g (π^*) SOMO

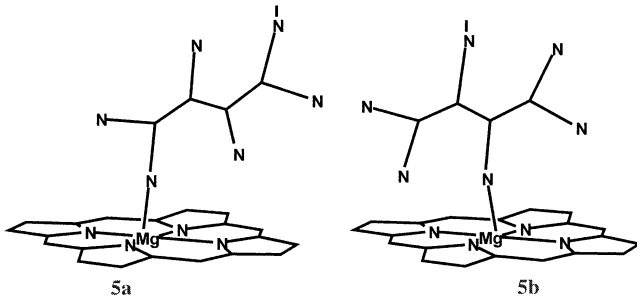

5a **5b**

The anomalously stronger antiferromagnetic coupling for **2** is also attributed to the interaction of the SOMOs in which the delocalized unpaired electron spin on the $[Mg^{II}(por^{\bullet})]^+$ and the $[TCNQF_4]^{\bullet-}$ reside. This overlap, however, is significantly greater than that for **1a** and **1b** as the 46.6° dihedral angle between the mean $[TCNQF_4]^{\bullet-}$ and $[Mg^{II}(por^{\bullet})]^+$ planes is substantially reduced 87° (Figure 8b). The closest contacts for **2** arise between the $C-C(CN)_2$ and the por$^{\bullet}$ plane that range from 3.38 to 4.70 Å. These contacts have a favorable orientation of the orbitals for overlap due to a small dihedral angle of 46.6° (Figure 8d). Furthermore, the 141.3° MgNC angle is ~26° less than that for **1a** and **1b** and positions the $[TCNQF_4]^{\bullet-}$ closer to the $[Mg^{II}(por^{\bullet})]^+$ plane (Figures 8b, 9b), which leads to an enhanced antiferromagnetic coupling. As a consequence, the susceptibility is reduced and is difficult to measure. On the basis of the given SOMO, orbital overlap is most significant between the $C_{(CN_2)}$ of $[TCNQF_4]^{\bullet-}$ and the *meso*-C of the porphyrin (Figure 9a). Furthermore, unlike for **1a** and **1b**, the $[TCNQF_4]^{\bullet-}$ F···por$^{\bullet}$ plane interaction is not present, and since the Mg lacks spin, the dominating $d_{z^2}/p_z(\pi_z)$ overlap (Figure 9a) is not present.

While the structures of the $[C_4(CN)_6]^{\bullet-}$-containing materials could not be determined, both *trans*-1,4-μ-N-bonding (**5a**) and interior *trans*-2,3-μ-N-bonding (**5b**) have been structurally characterized for $[MnOEP][C_4(CN)_6]$[41] (H_2OEP = octaethylporphyrin) and $[MnTBuPP][C_4(CN)_6]$[27j] [H_2TBuPP = tetrakis(4-*tert*-butylphenyl)porphyrin], respectively, and other geometries can occur. As the $[C_4(CN)_6]^{\bullet-}$ spin is delocalized and resides in the SOMO,[27j] in any of these geometries it should interact with the spin in the a_{2u} SOMO of the $[Mg(por^{\bullet})]^+$ again leading to antiferromagnetic coupling. As already discussed, the degree of overlap increases with decreasing dihedral angle between the mean MgN_4 and $[TCNQF_4]^{\bullet-}$ planes, and the stronger coupling for **4** (like **2**), with respect to **3** (like **1a** and **1b**), is attributed to a reduced dihedral angle. This occurs for the structurally characterized **1a**, **1b**, and **2** (and its isomorphous Mn analogue[24]), as well as several other 3,5-disubstituted [MnTPP][TCNE] materials;[3a,10,27n,42] hence, it is expected to occur for **4** with respect to **3**.

Conclusion

Despite having 1-D chain structural similarities, and **2** even being isomorphous to its Mn analogue, the magnesium and manganese porphyrin electron transfer complexes with strong cyanocarbon acceptors have very different magnetic properties. Both display paramagnetic behavior at room temperature; however, the members of the $[Mn(por)]^+$ family exhibit strong antiferromagnetic coupling and order as ferrimagnets at low temperature, while the members of the $[Mg(por^{\bullet})]^+$ family have only weak antiferromagnetic interactions. These differences in magnetic properties can be attributed to the site of oxidation. Manganese porphyrins undergo oxidation at the metal center, forming $S = 2$ Mn^{III} upon oxidation with $TCNQF_4$; hence, the spins are primarily located on the metal ion site. In contrast, $Mg^{II}(por)$ undergoes oxidation on the porphyrin ring producing a π-cation radical, i.e., $[Mg^{II}(por^{\bullet})]^+$, and lacks spin at the metal ion site. With the unpaired electron located on the porphyrin ring, it interacts with the unpaired electron spin residing on the radical anion of the electron acceptor, leading to antiferromagnetic coupling. The antiferromagnetic coupling increases as the $[Mg^{II}(por^{\bullet})]^+$ and $[TCNQF_4]^{\bullet-}$ get closer as evidenced by a decreased MgNC and dihedral angles between the mean MgN_4 and the mean $[TCNQF_4]^{\bullet-}$ planes.

The π-cation radicals observed for magnesium(II) tetraarylporphyrins are also present in copper(II) tetraarylporphyrins. In the latter case, $S = {}^1/_2$ d^9 Cu^{II} has one spin on the metal center, and electron transfer would occur from the porphyrin ring to the acceptor ligand. Hence, oxidation would be spin interactions between the $S = {}^1/_2$ copper site, $S = {}^1/_2$ π-cation porphyrin radical, and $S = {}^1/_2$ electron acceptor radical anion. Previous studies[43] of isolated copper(II) porphyrin radical cation systems such as $[Cu(TMP)][SbCl_6]\cdot C_6H_5F$ (H_2TMP = tetramesitylporphyrin) suggest a paramagnetic $S = 1$ triplet ground state for $[Cu^{II}(por^{\bullet})]^+$. The synthesis of $[CuTPP][TCNQF_4]$ or $[CuTPP][C_4(CN)_6]$ is, however, not thermodynamically favorable due to the need of a stronger reducing agent than is available; thus, this system was not studied.

(41) Miller, J. S.; Vazquez, C.; Jones, N.; McLean, R. S.; Epstein, A. J. *J. Mater. Chem.* **1995**, *5*, 707.
(42) Miller, J. S.; Brandon, E. J. In *NATO ARW Supramolecular Engineering of Synthetic Metallic Materials: Conductors and Magnets*; Veciana, J., Rovira, C., Amabilino, D., Eds.; 1998; Vol. C518, p 197. Kluwer Academic Publishers, Dordrecht.
(43) Erler, B. S.; Scholz, W. F.; Lee, Y. J.; Scheidt, R.; Reed, C. A. *J. Am. Chem. Soc.* **1987**, *109*, 2644.
(44) Baudron, S. A.; Mézierè, Heuzé, K.; Fourmigué, M.; Batail, P.; Molinié, P.; Auban-Senzier, P. *J. Solid State Chem*., in press.
(45) Miller, J. S.; Zhang, J.; Reiff, W. M. *J. Am. Chem. Soc.* **1987**, *109*, 4584.
(46) Rittenberg, D. K.; Sugiura, K.-i.; Arif, A. M.; Sakata, Y.; Incarvito, C. D.; Rheingold, A. L.; Miller, J. S. *Chem. Eur. J.* **2000**, *6*, 10, 1811.

Acknowledgment. The authors gratefully acknowledge the support in part from the National Science Foundation Grants CHE9730948, CHE 0110685, and CHE-9002690 and the University of Utah Institutional Funds Committee, Trent D. Selby for the synthesis of $C_4(CN)_6$, and Marc Fourmigué and Stéphane Baudron for a preprint of their work cited in ref 44.

IC020494W